The Journal of Experimental Biology 214, 3935-3947

doi:10.1242/jeb.058461

RESEARCH ARTICLE

Changes in wingstroke kinematics associated with a change in swimming speed in a pteropod mollusk, *Clione limacina*

Brett G. Szymik[1,*] and Richard A. Satterlie[2]

[1]Department of Biological and Environmental Sciences, Longwood University, Farmville, VA 23909, USA and [2]Department of Biology and Marine Biology and Center for Marine Science, University of North Carolina, Wilmington, NC 28409, USA

*Author for correspondence (szymikbg@longwood.edu)

Accepted 5 September 2011

SUMMARY

In pteropod mollusks, the gastropod foot has evolved into two broad, wing-like structures that are rhythmically waved through the water for propulsion. The flexibility of the wings lends a tremendous range of motion, an advantage that could be exploited when changing locomotory speed. Here, we investigated the kinematic changes that take place during an increase in swimming speed in the pteropod mollusk *Clione limacina*. *Clione* demonstrates two distinct swim speeds: a nearly constant slow swimming behavior and a fast swimming behavior used for escape and hunting. The neural control of *Clione*'s swimming is well documented, as are the neuromuscular changes that bring about *Clione*'s fast swimming. This study examined the kinematics of this swimming behavior at the two speeds. High speed filming was used to obtain 3D data from individuals during both slow and fast swimming. *Clione*'s swimming operates at a low Reynolds number, typically under 200. Within a given swimming speed, we found that wing kinematics are highly consistent from wingbeat to wingbeat, but differ between speeds. The transition to fast swimming sees a significant increase in wing velocity and angle of attack, and range of motion increases as the wings bend more during fast swimming. *Clione* likely uses a combination of drag-based and unsteady mechanisms for force production at both speeds. The neuromuscular control of *Clione*'s speed change points to a two-gaited swimming behavior, and we consider the kinematic evidence for *Clione*'s swim speeds being discrete gaits.

Key words: *Clione limacina*, flapping flight, kinematics, pteropod, speed change, swimming.

INTRODUCTION

Animals that locomote using flexible appendages may not be as easily modeled as those that locomote using rigid structures, but the two groups share certain characteristics. The rhythmic movement of locomotory appendages is a common trait, and soft-bodied invertebrates have proven invaluable for studying the neural generation and control of rhythmic locomotory behaviors (Arshavsky et al., 1985a; Harris-Warrick and Marder, 1991; Satterlie, 1985; Trimmer and Issberner, 2007; Watson et al., 2002; Willows and Hoyle, 1969). In addition to rhythmic movement of appendages, many locomotory systems share the ability to change speed. Soft-bodied invertebrate preparations have been used to study the neural control of speed changes at the cell (Antzoulatos and Byrne, 2007; Satterlie et al., 2000), neural network (Arshavsky et al., 1985b; Arshavsky et al., 1989; Ormshaw and Elliott, 2006; Satterlie, 1991b; Satterlie and Norekian, 1995) and behavioral levels (Seibel et al., 1998; Quillin, 1999).

This project used a molluskan preparation to examine how flexible appendages can produce meaningful locomotion and how these appendages can produce a pronounced change of speed. *Clione limacina* is a pteropod mollusk (pteropod means 'winged foot'), and like all pteropods, *Clione* rhythmically flaps two highly modified foot structures called parapodia (hereafter, 'wings'). These wings give pteropods the common name 'sea butterflies'. *Clione* is often called the 'sea angel', earning this moniker because of its upright body orientation. Its outstretched wings lie in the medial–lateral plane and flap dorsal–ventrally, producing movement in the rostral (superior) direction. This wing motion forces water downwards such that forward locomotion is movement up the water column to shallower depths. *Clione*'s flexible wings are mechanically supported solely by their own tissues and by the animal's hydrostatic skeleton.

Clione is both pelagic and negatively buoyant. To maintain its position in the water column, it demonstrates a slow swimming behavior. But when *Clione* is perturbed or when it is hunting, it enters into a fast swimming speed. The transition from slow to fast swimming is often triggered by a startle response, and can be reliably elicited experimentally by touching the animal's tail. *Clione* swims at a Reynolds number (*Re*) around 100, placing it at the low end of the intermediate flow regime (Daniel et al., 1992). As such, the flow of fluid around *Clione*'s wings is expected to be transitional, exhibiting both laminar and mildly turbulent flow. *Clione*'s *Re* allows comparison of its flapping swimming with the deep literature on low *Re* flapping flight, notably in *Drosophila*.

With distinct locomotory speeds, *C. limacina* is an ideal candidate for the study of speed changes. This is in contrast to the highly similar species *Clione antarctica*. *Clione antarctica*'s morphology is like that of *C. limacina*, but it does not exhibit fast swimming behavior or the strong startle response of *C. limacina*. Borrell and colleagues did not observe this behavior in any of 400 *C. antarctica* animals (Borrell et al., 2005), and Gilmer and Lalli report that *C. antarctica* both swims more slowly than *C. limacina* and responds to stimuli by cessation of swimming rather than escape (Gilmer and Lalli, 1990). The global distribution of *C. limacina* and *C. antarctica*

appears to be circumpolar, with *C. limacina* occupying the northern hemisphere and *C. antarctica* occupying the southern hemisphere, primarily in the Antarctic Circle (Gilmer and Lalli, 1990). Because *C. antarctica* does not demonstrate the two distinct swimming speeds seen in *C. limacina*, this project focused entirely on *C. limacina*, henceforth simply referred to as *Clione*.

Clione's wing flapping is controlled by a central pattern generator (CPG), which consists of two groups of neurons that fire out of phase. One group initiates upstroke, the other downstroke. Rhythmic activity in the two groups of neurons results from reciprocal inhibition combined with post-inhibitory rebound (Arshavsky et al., 1985a; Satterlie, 1985; Pirtle and Satterlie, 2004). Slow swimming arises from the interneurons of the swim CPG stimulating motoneurons that innervate slow twitch muscle fibers in the wings (Satterlie, 1991a). During fast swimming, the swim CPG is reconfigured by type 12 interneurons (Arshavsky et al., 1985b; Arshavsky et al., 1989), and there is recruitment of large diameter motoneurons that innervate both slow and fast twitch muscle in the wing (Satterlie, 1991b; Satterlie, 1993). Serotonin causes spike narrowing in the swim CPG cells, increasing their firing rate (Satterlie et al., 2000). The transition from slow to fast swimming arises from distinct modification of the swim CPG's behavior such that, neurologically, *Clione*'s swimming is very much a two-geared system.

From a neuromuscular standpoint, *Clione*'s transition from slow to fast swimming resembles a gait transition. Distinct changes take place to effect an increase in speed: neural pathways are modified and more and different muscle fibers are recruited. While different gaits may exist to minimize energy expenditure (Hoyt and Taylor, 1981), studies have routinely examined gaits using kinematic measures. Discrete gaits have been defined solely by the timing or duration of kinematic events, e.g. the terrestrial walk/run transition has been defined across species as occurring when a limb's duty factor falls below 50%, duty factor being the phasic length of time that the foot is in contact with the ground (Hildebrand, 1965). However, not all locomotory systems that exhibit gaits are so easily defined; gait changes in some birds are smooth (Gatesy and Biewener, 1991).

Satterlie and Norekian note three mechanisms by which *Clione* increases its swimming speed: (1) it increases wingbeat frequency, (2) it increases the force of wing movement by recruiting muscle fibers and changing the duration and intensity of contraction, and (3) it changes 'biomechanical aspects' of its wingbeat (Satterlie and Norekian, 2001). Beyond describing the kinematics of *Clione*'s swimming, the present study primarily addresses point 3 by comparing the kinematics of *Clione*'s wingbeat during slow and fast swimming and observing differences outside of wingbeat frequency (point 1). There is tremendous evidence that *Clione* has adapted physiologically to produce two swimming speeds. This study characterized the kinematics of *Clione*'s swimming at both slow and fast speeds to determine whether the physiological characteristics attributed to producing fast swimming are accompanied by phasic changes in how the animal moves.

MATERIALS AND METHODS

Individual *C. limacina* (Phipps 1774) were collected from the surface water off the breakwaters at the University of Washington's Friday Harbor Laboratories (Friday Harbor, WA, USA). The animals were kept in gallon-sized glass jars filled with fresh, filtered seawater that was changed twice daily. The temperature of the jars was maintained by immersing them in sea tables filled with flowing seawater pumped from the harbor. *Clione* were fed their natural prey, *Limacina helicina*, if specimens were found, but no formal feeding schedule was maintained. Animals were filmed within days of collection.

Animal preparation

Animals were filmed in a Plexiglas container composed of two chambers. One chamber was filled with fresh, filtered seawater into which animals were placed for filming, and had dimensions of 15×18.5×13 cm. These dimensions were presumed large enough relative to animal size to exclude wall effects, and animals were placed in the center of the chamber when filmed. The second chamber abutted the filming chamber and held an ice-water bath. This chamber cooled the filming chamber as *Clione* often ceases to swim if the water temperature rises. The ice bath was maintained, but the temperature of the water in the filming chamber was not otherwise regulated.

To allow the filming of multiple consecutive wingbeats, and to allow the filming of fast swimming behavior, some animals were tethered to a glass capillary tube mounted to a metal base. VetBond tissue adhesive (3M, St Paul, MN, USA) was used to glue the tip of the animal's tail to the glass tube. The animals were placed onto a clean surface and most of the seawater surrounding the tip of the tail was wicked away. Glue was applied to the glass pipette and the pipette held to the tip of the tail. VetBond polymerizes in seconds, and the animal (now attached to the tether) was immediately returned to the seawater bath. *Clione* were tethered by the tip of the tail to allow body movement yet minimize tethering effects. The tail's tip is the farthest point on the body from the wings, and the body is both highly flexible and not muscularly active in non-turning swimming behavior.

Animals were given ample time in the filming chamber to recover from the gluing procedure. All animals began swimming immediately after being returned to the water bath. Often, animals entered fast swimming, presumably as an escape response to tail stimulation. All animals slowed to normal swimming within 10 min. Fast swimming was elicited by touching the tip of the animal's tail with a probe. All animals showed a startle response, followed by a bout of fast swimming.

Filming of animal movement

The direct linear transformation (DLT) technique (Abdel-Aziz and Karara, 1971) was employed to obtain 3D data from video recordings. A pair of Redlake MotionMeter digital cameras (Tallahassee, FL, USA) were used to simultaneously film animals. Prior to filming each video sequence, a custom-built calibration object containing numerous metal spheres was inserted into the filming chamber and imaged in each camera. The centroid of each sphere was surveyed by Datum Inspection Services (Phoenix, AZ, USA) at the micrometer level. A minimum of 16 spheres were imaged and used to perform the DLT.

The cameras were placed at steep angles to the recording chamber where refractive effects due to the water–air interface would be minimal. After imaging the calibration object, the cameras were not adjusted. The calibration object was removed from the filming chamber and the animal was moved into the cameras' fields of view. Swimming behavior was recorded at 125 frames s^{-1} at full resolution, and a 10× digital shutter was employed to further freeze movement. The cameras were linked to ensure frame synchronization and a voltage step signal was sent to each camera to simultaneously stop recording. All frames from the two video sequences (one sequence from each camera) were captured onto a desktop computer in TIFF format *via* a μTech MV-510 frame-grabber board (captured at

658×496 pixels, 8-bit grayscale). Prior to analysis, the frames for each video were stacked and saved as an uncompressed AVI file.

Untethered animals were filmed using the same technique. *Clione* were allowed to swim freely about the filming chamber until they swam through the volume imaged by the cameras' fields of view. Because of the long focal lengths of the lenses, their shallow depths of field, and the low resolutions of the cameras, it was not possible to film an entire wingbeat of a fast swimming untethered *Clione*. Untethered slow swimming behavior was successfully recorded, though never for multiple consecutive wingbeats.

For 3D data, Peak Motus v.8 (Vicon, Los Angeles, CA, USA) was used to manually digitize movement in the videos and to perform the DLT transformation. Various landmarks on the body of the animal were manually digitized in each video frame. 3D data were rotated to define the outstretched wingtips at midstroke as the medial–lateral axis and the position of the head at midstroke as the origin. Movement data were smoothed using Motus' inbuilt Butterworth filter, and velocity and acceleration data were obtained from Motus' numerical differentiation of these smoothed data.

Because the trailing edge of the wing was occasionally obscured by the animal's body (as a result of its tremendous flexibility and range of motion), 2D body and wing angle measurements were made on a separate group of tethered animals. Animals were filmed with a single camera positioned laterally. Digitization was performed using a MATLAB (MathWorks, Natick, MA, USA) program (Hedrick, 2008). At midstroke, the center of the animal's head and the bottom of its gut (a high contrast landmark) were digitized, as were the leading and trailing edges of the wing. The wingtip was digitized through the midstroke, and linear regression (Microsoft Excel 2011) of these data defined the path of the wingtip as the stroke plane. A body coordinate system was defined (illustrated in Fig. 2). The body's rostral–caudal axis was defined by the head and gut points, and the dorsal–ventral axis was placed orthogonal to this. Wing chord was defined by the leading and trailing edges' points. The angle of attack of the wing, α, was defined as the angle between the wing chord and the stroke plane. The stroke plane angle, β, was defined by the wingtip's path and the body's dorsal–ventral axis. The chord angle of the wing, γ, was defined by the wing chord and the body's dorsal–ventral axis.

Numerical data were output from Motus and MATLAB and statistical analyses were performed using Origin v.7.5 (OriginLab, Northampton, MA, USA) or Excel. Student's *t*-tests were used to compare means. Means are reported ±1 s.d. Coefficient of variation was calculated as standard deviation divided by mean, and expressed as a percentage.

Morphometric measurements

After filming, animals were placed into a Petri dish of room temperature seawater. The warm temperature caused swimming cessation. A ruler was placed next to the animal and a digital photograph was taken holding the camera such that its sensor was parallel with the bench surface. Pixel distances were calibrated to the ruler and measurements were made using ImageJ. L, the length of a single wing, was measured as the wingspan from the wingtip to the base of the wing where it attaches to the body. The aspect ratio, AR, of the wing is equal to four times the squared wing length divided by wingspan, S ($=4L^2/S$). Wingspan (S) was calculated as $2L$, and was also measured directly as the distance from right wingtip to left wingtip including the width of the body (S^1). Wing chord (c) was measured from the leading edge to the trailing edge at the center of the wing's span. Mean wing chord ($\bar{c}$) is equal to the wing area divided by wingspan ($=A/S$). Wing surface area (A) was measured using ImageJ by tracing a polygon around the edges of the relaxed wing in the photograph and having the software calculate the calibrated area of the polygon.

Wingbeat frequencies were measured from the video sequences by counting the number of frames over one or more wingbeats. The number of wingbeats used to calculate wingbeat frequency varied from 1 to 10 depending upon video length.

The Reynolds number of the wing (Re) was calculated as the density of seawater times the mean peak velocity of the wingtip multiplied by the mean wing chord ($\bar{c}$), divided by the dynamic viscosity of seawater. The density of seawater was assumed to be $1028.106\,kg\,m^{-3}$ and the dynamic viscosity $1.892\times10^{-3}\,kg\,m^{-1}\,s^{-1}$, values for seawater at temperature 0°C and salinity $35\,g\,kg^{-1}$ (Haynes, 2010). The advance ratio, J, of untethered animals was calculated as the mean body velocity (indicated by the head) divided by mean peak wingtip velocity.

RESULTS

In *Clione*, one complete wingbeat cycle involves a dorsally directed upstroke, followed by a ventrally directed downstroke (Fig. 1). In anesthetized or non-swimming animals, the relaxed wings naturally

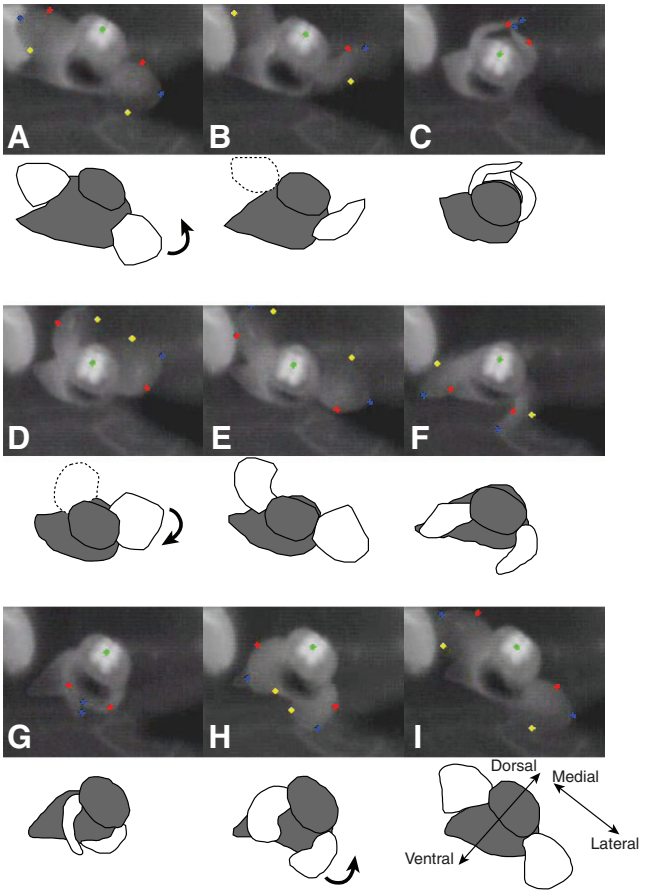

Fig. 1. Rostral (superior) and slightly ventral view of *Clione limacina* untethered slow swimming behavior. One complete wingbeat cycle is shown in video still frames (A–I). Line drawings under each frame show the animal's head and body in gray and wings in white. Wings that fell partially out of frame are shown as dashed lines. Colored dots are body landmarks digitized in each frame. (A,E,I) Wings maximally outstretched at midstroke; (C) maximum upstroke; (G) maximum downstroke. Green, center of head; red, leading edge; blue, wingtip; yellow, trailing edge; arrows, direction of wing movement.

Table 1. Morphometric data and kinematic variables for *Clione limacina*

Animal	L (mm)	AR	S (mm)	S^1 (mm)	c (mm)	$\bar{c}$ (mm)	A (mm^2)	n_s (Hz)	n_f (Hz)	Re_s	Re_f
1	3.35	5.16	6.70	8.50	3.39	3.29	8.7	1.65	2.67	47.7	67.6
2	4.82	6.64	9.64	11.95	4.65	3.87	14.0	2.00	2.54	79.6	109.8
3	3.71	5.24	7.42	10.02	4.34	3.71	10.5	2.10	3.18	190.1	318.6
4	4.34	5.75	8.68	10.41	4.87	4.16	13.1	2.37	2.80	237.3	308.6
5	6.49	5.93	12.98	17.03	6.69	5.66	28.4	1.82	–	191.1	–
6	7.37	5.61	14.74	16.87	8.11	6.84	38.7	1.82	–	88.6	–
7	7.28	7.11	14.56	15.83	7.30	6.12	29.8	1.44	–	197.0	–
8	7.66	4.92	15.32	19.36	9.14	7.78	47.7	1.14	–	186.0	–

Animals without fast swimming data were filmed untethered.

L, wing length; AR, aspect ratio; S, wing span; S^1, wing span from wingtip to wingtip including body; c, wing chord; $\bar{c}$, mean wing chord; A, surface area of one wing; n_s, slow swim wingbeat frequency; n_f, fast swim wingbeat frequency; Re_s, Reynolds number of the wing during slow swimming; Re_f, Reynolds number of the wing during fast swimming.

fall fully outstretched, with wingtips pointing laterally. Also, midstroke was more reliably timed in videos and kinematic traces than the stroke maxima. As such, the beginning of the wingbeat cycle was defined as the point when the wingtips were fully outstretched during upstroke (Fig. 1A). The middle of the wingbeat cycle (phase ~0.5) occurred when the wings were fully outstretched during downstroke (Fig. 1E).

As upstroke concludes, the wings are bent considerably along their span and wrap around the body (Fig. 1C). In some animals, left and right wingtips cross over at the stroke maxima. Downstroke begins, and the wings reverse direction, unwrap, and straighten along their span (Fig. 1D). Wing straightening is accompanied by rotation about the span, forming the angle of attack. As with upstroke, downstroke concludes with spanwise bending and the wings wrapping around the body's rostral–caudal (long) axis (Fig. 1G). Wing reversal occurs and upstroke begins with the wings straightening along their span and rotating spanwise to form the upstroke angle of attack (Fig. 1H). Peak wingtip velocity occurs at approximately the middle of each half-stroke, when the wings are fully outstretched (Fig. 1A,E,I; further discussed below).

Mean slow swimming wingbeat frequency, n_s, was 1.79±0.4 Hz, whereas fast swimming occurred with a mean frequency, n_f, of 2.80±0.3 Hz (Table 1). *Re* of the mean wing chord during slow swimming, Re_s, varied from 47.7 to 237 with a mean of 152±69. Fast swimming Re_f varied from 67.6 to 319, averaging 201±131. The advance ratio, J, of untethered animals varied from 0.16 to 0.70, while tethered animals had an advance ratio of zero because of their lack of ascent velocity.

The stroke plane angle, β (Fig. 2), averaged 12.3±5.1 deg during slow swimming downstroke and 9.8±4.4 deg during upstroke

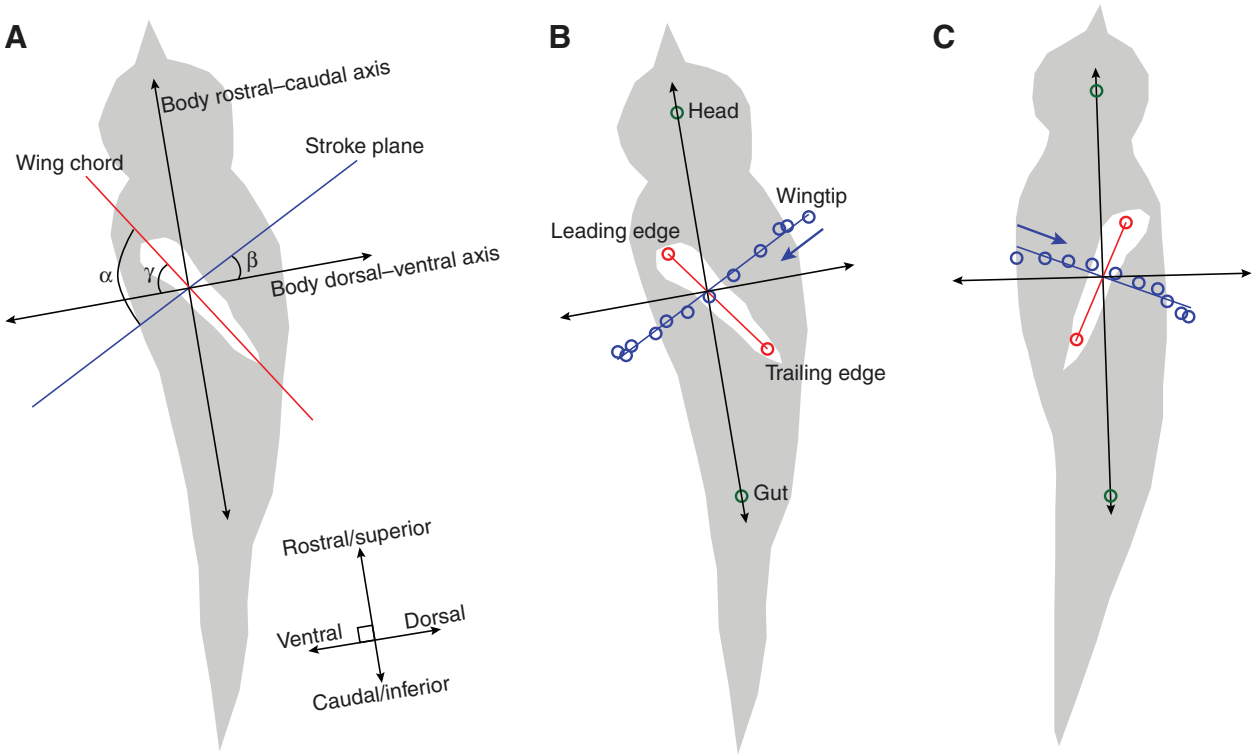

Fig. 2. Kinematic wing and body angles in a lateral view of *Clione* at midstroke. Gray, tracing of the body; white, wing. (A) α, angle of attack; β, stroke plane angle; γ, chord angle. (B) Downstroke, circles denote digitized points. The center of the head and bottom of the gut (green) define the body's rostral–caudal axis and the body's dorsal–ventral axis lies at a right angle to this. Leading and trailing edges of the wing (red) define the wing chord. A linear regression applied to the path of the wingtip through the power stroke defines the stroke plane (blue). Blue arrows, direction of wingtip movement. (C) Upstroke in same animal.

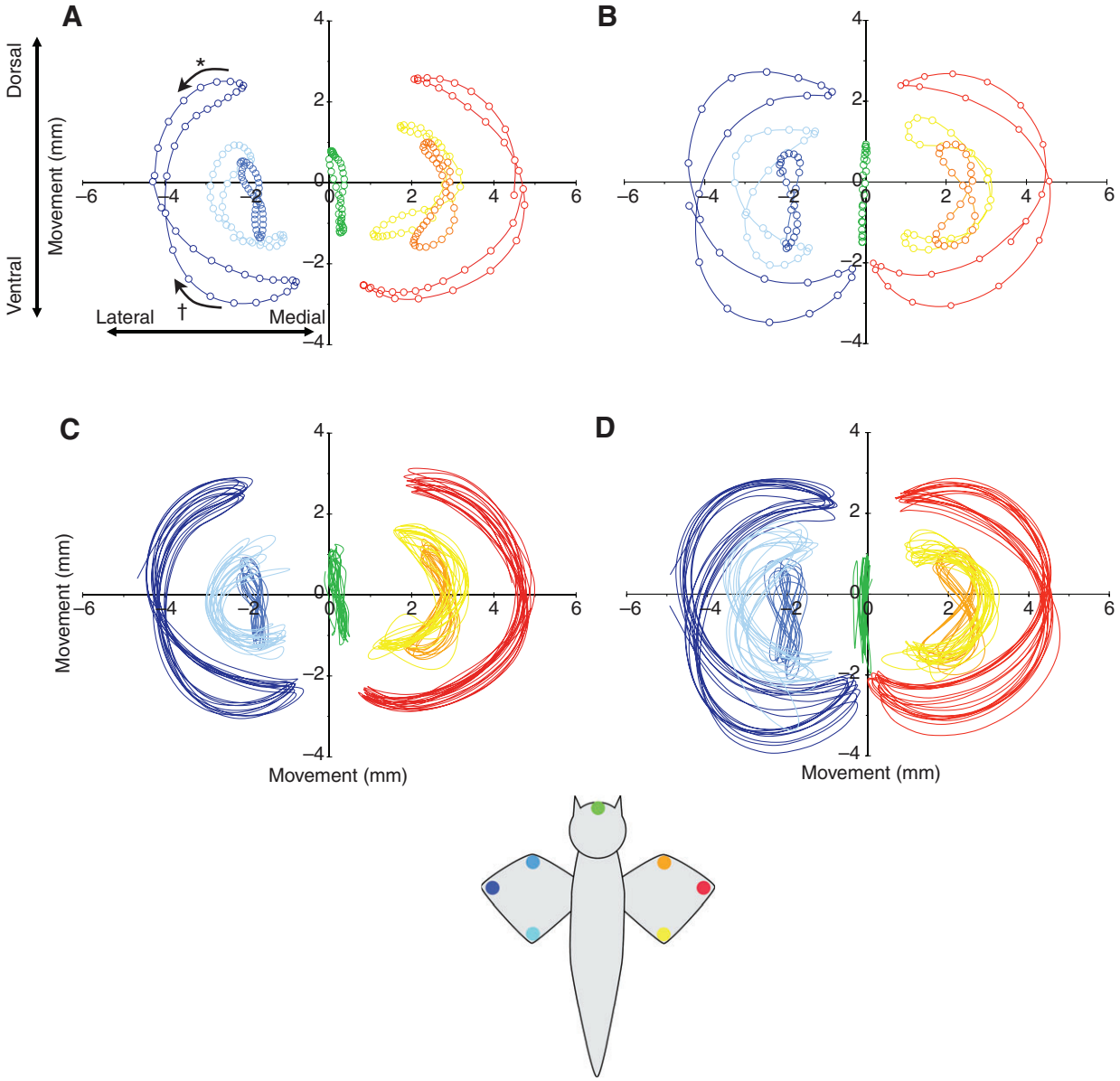

Fig. 3. Rostral (superior) view of tethered *Clione* swimming kinematics. Projecting the 3D data downwards shows movement along the dorsal–ventral/medial–lateral plane. The animal's head (green) was defined as the center of the coordinate system at midstroke. (A) One complete wingbeat during slow swimming. (B) One fast swimming wingbeat in the same animal. (C) Ten consecutive slow swimming wingbeats. (D) Ten fast swimming wingbeats. Inset: warm colors, right wing; cool colors, left wing; red and dark blue, wingtips; orange and light blue, leading edges; yellow and pale blue, trailing edges; *, direction of downstroke movement; †, direction of upstroke movement.

(N=40). β during fast swimming increased to 17.1±8.6 deg for downstroke and 15.5±3.8 deg for upstroke. Mean chord angle of the wing at midstroke relative to the dorsal–ventral axis of the body, γ, was 44.6±5.1 deg during slow swimming downstroke and 41.3±6.8 deg during upstroke. Satterlie and colleagues observed a similar slow swimming γ (reported as angle of attack): 42.5±5.2 deg during downstroke and 42.4±6.8 deg during upstroke (Satterlie et al., 1985). γ increased during fast swimming to 53.0±3.2 deg during downstroke and 47.4±9.0 deg during upstroke. The wing's angle of attack, α, averaged 63.9±5.2 deg during slow swimming downstroke and 59.2±6.9 deg during upstroke. α increased in fast swimming to 70.1±8.3 deg during downstroke and 63.0±10.6 deg during upstroke.

Projecting the 3D movement data onto the medial–lateral/dorsal–ventral plane provides a rostral (superior) view of swimming behavior (Fig. 3). The wingtips trace a folded figure-of-eight pattern through space, with greater extension of the wingtip away from the base of the wing during the beginning of each half-stroke (Fig. 3A, * and †).

Tethering animals allowed the filming of consecutive wingbeats and fast swimming behavior. Without tethering, upwards progression of the animal in the water column caused it to exit either the cameras' fields of view or the cameras' depths of field. Some animals were successfully filmed untethered while performing slow swimming, and their kinematics were compared with those of slow swimming tethered animals (Fig. 4).

A major concern with tethering was its possible effects on whole-body translation during swimming, aside from the obvious effect of negating upwards progression. The center of the head was

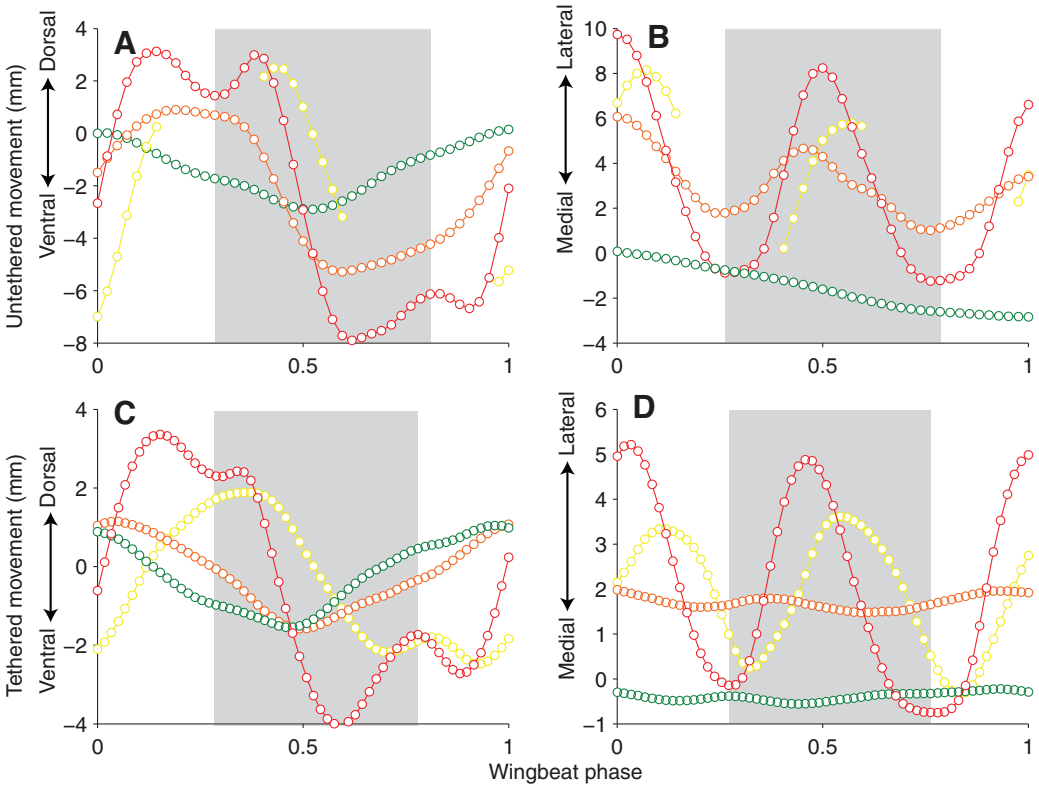

Fig. 4. Untethered (A,B) and tethered (C,D) slow swimming in *Clione*. (A) Untethered dorsal–ventral wing and head movement through a single wingbeat. (B) Untethered medial–lateral movement. (C,D) Tethered movement (different animal). Circles represent individual digitized points. Colors as in Fig. 3 inset: green, head; red, right wingtip; orange, leading edge; yellow, trailing edge. In A and B, the trailing edge was occasionally obscured by the animal's body in one or both cameras. Gray bars, downstroke.

digitized as a general indicator of body position. Untethered and tethered movement data show similar dorsal–ventral 'back-and-forth' patterns of head movement (Fig. 4A,C, green). During upstroke, the head moves ventrally as the wings move dorsally, then *vice versa* during downstroke. Over multiple wingbeats, the head oscillates back and forth in the dorsal–ventral plane in both untethered and tethered animals. Borrell and colleagues saw an analogous pattern of head movement in freely swimming *C. antarctica*, which they described as a 'saw-toothed path' as the animal progresses up the water column (Borrell et al., 2005).

Tethering by the tip of the tail has the potential to alter the body's back-and-forth translation into a rotational motion about the tether attachment, so head movement was compared between tethered and untethered animals. The amplitude of each animal's dorsal–ventral head movement was measured over multiple wingbeats and averaged. The amplitude of head movement is likely influenced by animal morphology and wing speed, so averages were divided by various parameters to normalize each individual's data for group comparison between tethered and untethered animals. Normalizing dorsal–ventral head movement to wingspan, S, showed no difference between tethered and untethered animals (P>0.36). This was also true when normalizing head movement to mean wing chord, $\bar{c}$ (P>0.30). Normalizing head movement to a key kinematic parameter, mean peak wingtip velocity during upstroke, similarly showed no significant difference between tethered and untethered animals (P>0.106).

All animals showed greater dorsal–ventral head movement during fast swimming, increasing from 2.22 mm during slow swimming to 2.42 mm during fast swimming (P<0.0498). Among tethered animals, dorsal–ventral head velocity was statistically similar during upstroke and downstroke. For head movement during the upstroke, the ventrally directed head velocity peaked at a mean of 14.3±7.69 mm s^{-1}, while during the downstroke, the dorsally directed velocity was statistically similar at 15.1±8.84 mm s^{-1} (P>0.32). During fast swimming, upstroke head velocity increased to 16.6±7.55 mm s^{-1} and downstroke head velocity increased to 19.4±9.16 mm s^{-1}, but they remained similar to each other within the speed (P>0.069). Head accelerations showed no difference (P>0.29) between upstrokes and downstrokes during slow swimming at 599.6±467 and 671.8±570 mm s^{-2}, respectively. However, during fast swimming, upstroke and downstroke head acceleration differed from one another (P<0.030). The upstroke ventrally directed head acceleration peaked at 741.7±318 mm s^{-2}, while downstroke produced a greater dorsally directed head acceleration at 945.8±474 mm s^{-2}. (Normalizing all of these amplitudes to each individual's S did not change the significance of the comparisons above/below critical values.)

As the wings reach their stroke maximum and begin reversal, the wingtips are pulled towards the body along the dorsal–ventral axis. Traces of dorsal–ventral wingtip movement show twin peaks about the stroke maxima, with the stroke maximum centered on the trough between peaks (Fig. 4A,C, red). The first peak is formed as the wingtip moves through the half-stroke and then bends about its span approaching the stroke maximum. This motion pulls the wingtip close to the body, forming a trough in the trace at the stroke maximum. The wing reverses motion and begins the next half-stroke, straightening along its span and forming the second peak. (This sequence can be seen in Fig. 1F–H, showing wing reversal, wingtips

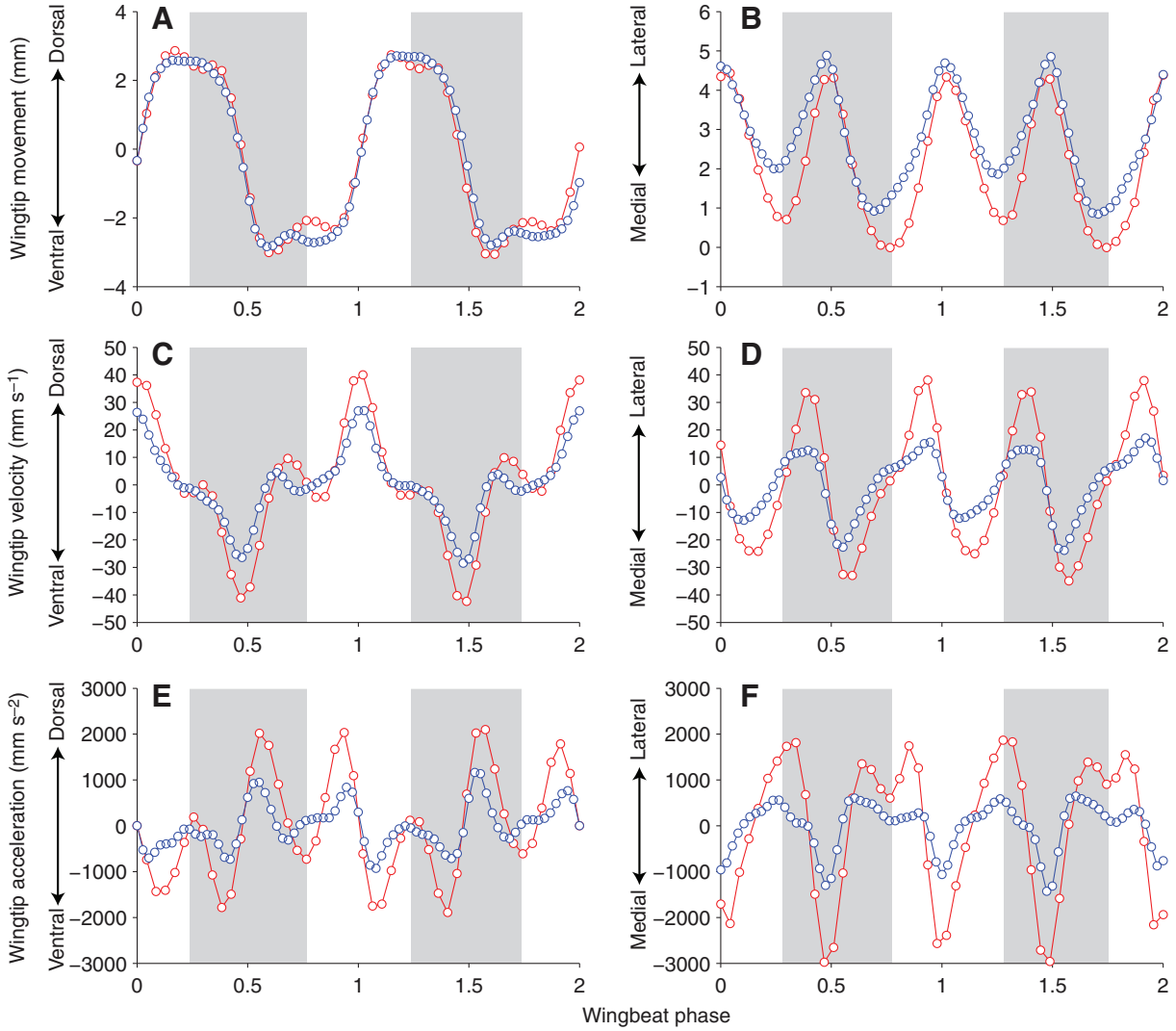

Fig. 5. (A) Dorsal–ventral wingtip movement through two consecutive wingbeats during slow swimming (blue) and fast swimming (red). (B) Corresponding medial–lateral wingtip movement. (C,D) Wingtip velocities in dorsal–ventral and medial–lateral directions. (E,F) Wingtip accelerations in dorsal–ventral and medial–lateral directions. Gray bars, downstroke.

blue.) While the magnitude of these twin peaks varies from animal to animal, the pattern is characteristic of both untethered and tethered wingtip movement during both upstroke and downstroke.

Wingtip movement along the medial–lateral axis has a roughly sinusoidal pattern in both untethered and tethered animals. Peaks in the trace (Fig. 4B,D, red) occur as the wings are fully outstretched and therefore the wingtips are in their most lateral position (as in Fig. 1A,E,I). Troughs in the trace occur at the stroke maxima as the wingtips approach, or even cross, the midline of the body and begin reversal (as in Fig. 1C,G). Troughs in medial–lateral wingtip traces are wider than peaks because maximum wingtip velocity occurs as the wings are outstretched.

Overlaying slow and fast swimming kinematics as a function of wingbeat phase highlights differences between swim speeds (Fig. 5). The most pronounced difference in dorsal–ventral wingtip movement (Fig. 5A) occurs at the stroke maxima as the wingtips come slightly closer to the body. Medial–lateral wingtip movement shows more dramatic differences with speed change (Fig. 5B). The wingtips more closely approach the body's midline during fast swimming, indicated by troughs near or below zero.

Peak dorsal–ventral velocity of the wingtips occurs at midstroke, when the wings are maximally outstretched (Fig. 5C). Peak upstroke wingtip velocity averaged 64.1±34.7 mm s^{-1} for slow swimming and 93.7±53.4 mm s^{-1} during fast swimming, a 46% increase. Peak downstroke wingtip velocity averaged 60.9±30.3 mm s^{-1} for slow swimming and 98.0±58.0 mm s^{-1} during fast swimming, a 61% increase. Wingbeat frequency increased by a mean of 39.4±17.7% from slow to fast swimming.

During wing reversal, spanwise bending is pronounced and the wingtips are pulled close the body (the 'twin peak' wingtip pattern noted above, as in Fig. 4A,C). As the wings straighten along their span and open following reversal, wingtip movement is momentarily in the direction opposite to that of the half-stroke. As a result, smaller secondary peaks in dorsal–ventral wingtip velocity traces occur shortly before and after wing reversal (Fig. 5C), and become larger during fast swimming. This pattern is more pronounced in wingtip acceleration traces (Fig. 5E) as each half-stroke shows both a dorsally directed peak and a ventrally directed one. During downstroke, the ventrally directed (negative) acceleration precedes the dorsally directed (positive)

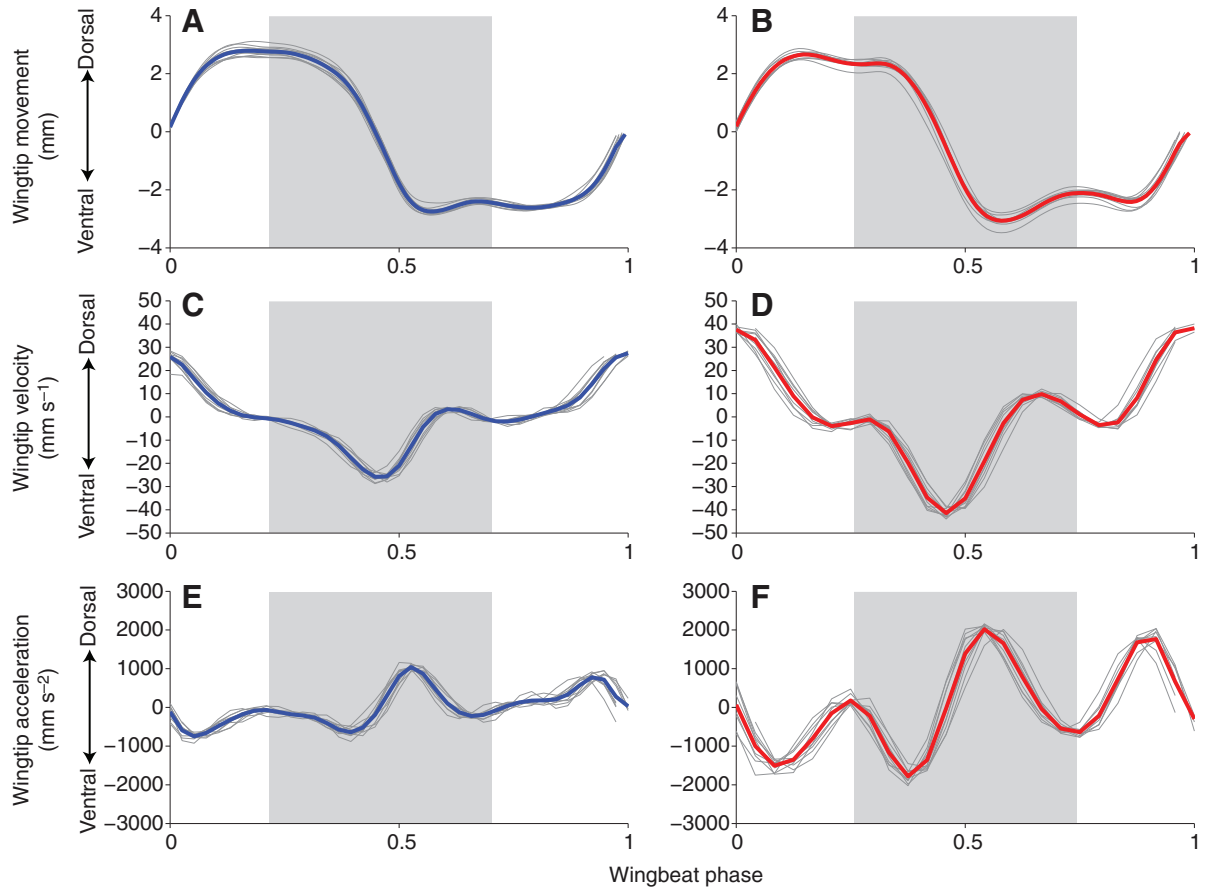

Fig. 6. (A) Dorsal–ventral wingtip movement during tethered slow swimming. Ten consecutive wingbeats from a single animal are overlaid (thin gray lines) and the mean value from these wingbeats is shown (thick blue line). (B) Fast swimming, mean displayed in red. (C,D) Dorsal–ventral wingtip velocity during slow and fast swimming. (E,F) Dorsal–ventral wingtip acceleration during slow and fast swimming. Gray bars, downstroke.

peak, while upstroke has a dorsal acceleration peak prior to a ventral one.

As a half-stroke begins, the wings straighten along their span. This movement of the wingtips away from the midline of the body is seen as a lateral-direction velocity peak (Fig. 5D), with a mean of 30.0±5.89 mm s^{-1} during slow swimming and a significant increase to 38.6±5.04 mm s^{-1} during fast swimming. As the half-stroke ends, the wingtips are pulled back towards the midline, causing a medial-direction (negative) velocity peak, averaging 31.4±14.0 mm s^{-1} during slow swimming and increasing significantly to 44.8±7.85 mm s^{-1} during fast swimming. During a single half-stroke, medial–lateral wingtip velocity therefore peaks immediately after the start of the half-stroke and immediately prior to the end of the half-stroke, and is zero when the wings are outstretched. Indicative of the curvature of the wingtip's path (Fig. 3), medial–lateral wingtip velocity is zero at the same time that dorsal–ventral wingtip velocity peaks.

The fast swimming acceleration pattern closely resembles the slow swimming pattern, with an expected increase in amplitude (Fig. 5E,F). The dorsal–ventral acceleration pattern is best described as a pair of ventrally directed peaks, followed by an analogous pair of dorsally directed peaks (Fig. 5E). Each peak in the pair is separated by a trough that crosses zero acceleration, centered on the timing of wing reversal. Between each pair of peaks, acceleration crosses zero as the wings hit their midstroke velocity peak. Medial–lateral acceleration shows a more complex pattern (Fig. 5F). Acceleration changes are sharpest before and after midstroke as the wings are outstretched and then are pulled back towards the midline of the body.

Overlaying data from consecutive wingbeats shows that the kinematics of the wingtips vary little within a speed. Fig. 6 overlays 10 consecutive wingbeats from the same animal during slow and fast swimming. Variation in wingtip movement (Fig. 6A,B) from beat to beat occurs mostly around the stroke maxima. The large variability in mean wingtip velocity reported above is primarily accounted for by variability between individuals; each individual's peak wingtip velocity varies little from wingbeat to wingbeat within a swim speed (Fig. 6C,D). The individual with the highest variability in velocity had a mean peak wingtip velocity of 157±17.9 mm s^{-1} during its fast swimming upstroke, a coefficient of variation of 11.4%. Yet, the smallest variation from the group data came during slow swimming downstroke, where mean peak wingtip velocity was 60.9±30.3 mm s^{-1}, a coefficient of variation of 49.8% (the highest was 59.2% during fast swimming downstroke).

Video still frames of the stroke maxima reveal how spanwise wing bending is more pronounced during fast swimming. Left and right wingtips either more closely approach each other or cross over at wing reversal during fast swimming as opposed to slow swimming (Fig. 7). Of the individuals in this study wherein both slow and fast swimming were reliably recorded, one individual's wingtips simply came closer together during fast swimming (Fig. 7A). In all other individuals, the wings wrapped around the body during fast

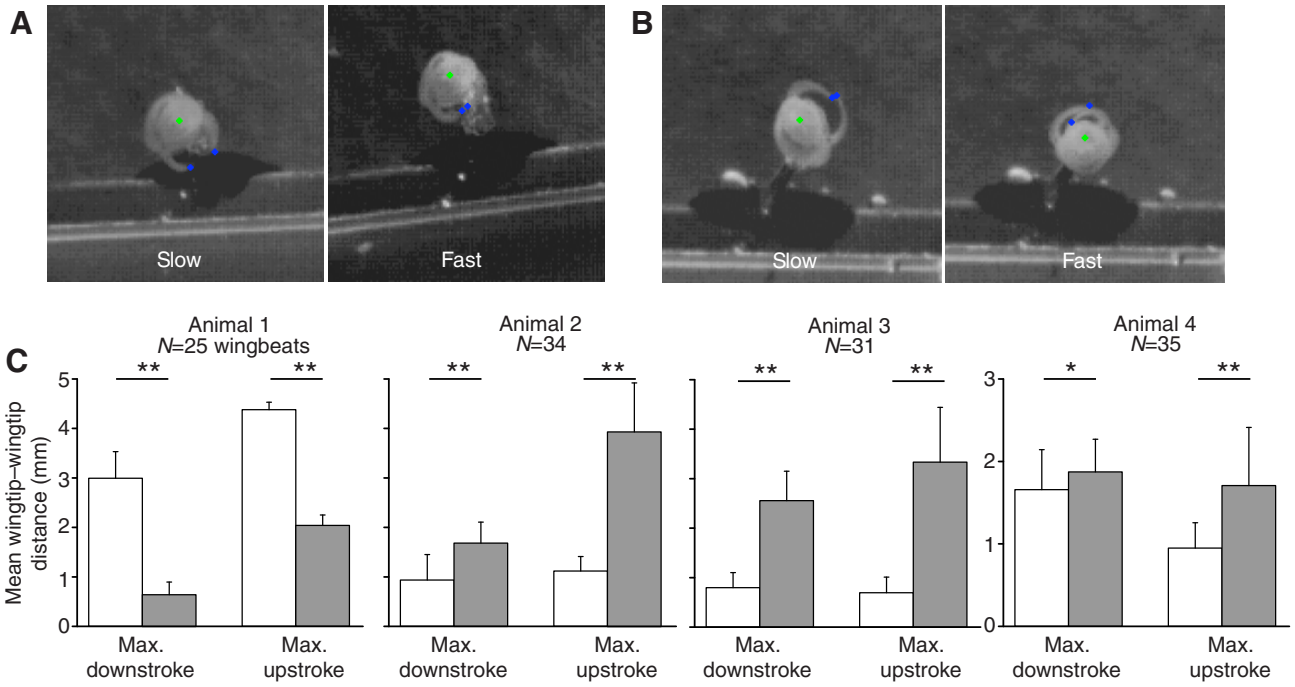

Fig. 7. Wingtip positions at the stroke maxima during slow and fast swimming. (A,B) Video still frames showing superior views of tethered *Clione* at maximum downstroke. (A) Wingtips are closer together at the stroke maxima during fast swimming. (B) Wingtips cross over during fast swimming in a different animal. Green, digitization of head position; blue, digitization of wingtips. (C) Mean absolute 3D distance between left and right wingtips during slow swimming (white bars) and fast swimming (gray bars) at maximum upstroke and maximum downstroke (i.e. wing reversal). Animal 1 shows a decrease in the distance between its wingtips during fast swimming, as in A. Animals 2–4 show an increase in the absolute distance between wingtips during fast swimming as the wings cross over, as in B. **P*<0.05; ***P*<0.001, two sample paired *t*-test comparing slow with fast swimming; error bars, 1 s.d.

swimming such that they crossed over at the stroke maxima (as in Fig. 7B). In animal 1, where crossing over did not occur, the mean absolute distance between the wingtips decreased significantly during fast swimming as the wingtips more closely approached each other (Fig. 7C). In animals 2–4, where crossing over did occur, the mean absolute distance between the wingtips increased significantly during fast swimming, indicative of the wingtips crossing over (at which time tip–tip distance was zero) and then continuing past each other before reaching the stroke maximum (Fig. 7C). This pattern of increased spanwise bending during fast swimming occurred during both upstroke and downstroke. In time-based kinematic traces, this pattern is most clearly seen in the medial–lateral plane as increased wingtip excursion towards the midline of the body during fast swimming (Fig. 5B).

Timing the beginning and end of each wingbeat allows for the phasic timing of other events relative to the wingbeat cycle (Fig. 8). As noted above, the midpoint of upstroke was chosen as the beginning of a wingbeat, and the next consecutive mid-upstroke as the end of that beat. During slow swimming, maximum upstroke occurred at 17.7±6.5% of the wingbeat phase, while it occurred significantly later in the cycle during fast swimming, at 24.5±3.4% (for all events, *N*=38 or 39 at each speed from 4 animals). Maximum downstroke showed a similar significant lag, moving from 72.1±5.1% of the wingbeat during slow swimming to 75.2±3.4% in fast swimming. Downstroke therefore occupied 54.4% of the slow swimming wingbeat and 50.7% of the fast swimming beat. Peak downstroke wingtip velocity occurred at 41.3±8.7%, immediately after mid-downstroke (40.5±6.7%). In fast swimming, this was delayed to 46.8±3.4% of the wingbeat, but remained similar to the timing of the fast swim mid-downstroke (44.7±3.5%). Dorsally directed wingtip velocity peaked at 1.1±1.4% after the middle of the upstroke (itself defined as 0), and during fast swimming it remained similarly timed at 0.8±1.9%. As the wingtips hit peak dorsal–ventral velocity, the velocity of the head peaked shortly afterwards, in the opposite direction.

DISCUSSION

The kinematics of *Clione*'s left and right wings show a high degree of symmetry. This symmetrical movement balances forces about the medial–lateral axis of the body and prevents angular alterations in trajectory, i.e. turning or spinning. The morphology of *Clione*'s tail may serve to decrease hydrodynamic drag, but the long, flattened tail likely also acts as a rudder to further stabilize movement along the body's long axis. Turning is actively accomplished by contractions of body wall musculature that cause tail bending (Deliagina et al., 1998). To that end, observing left/right wing kinematic symmetry is unsurprising as none of the animals filmed in this study were engaged in turning maneuvers.

However, in steady, non-turning swimming, translation of the body occurs. In tethered animals, this was observed as dorsal–ventral movement of the head (Figs 3 and 4). As the wings approach the mid-point of their half-stroke and are almost fully outstretched, the horizontal component of their force production causes the head to move in the opposite direction along the dorsal–ventral axis (Fig. 4), its velocity peaking shortly after that of the wingtips (Fig. 8). Consecutive wingbeats cause a back-and-forth translation of the body. This dorsal–ventral whole-body translation is balanced in each half-stroke such that untethered animals that swim upwards show a zig-zag progression – in both slow and fast swimming – but their overall trajectory remains in the rostral direction. Slow swimming

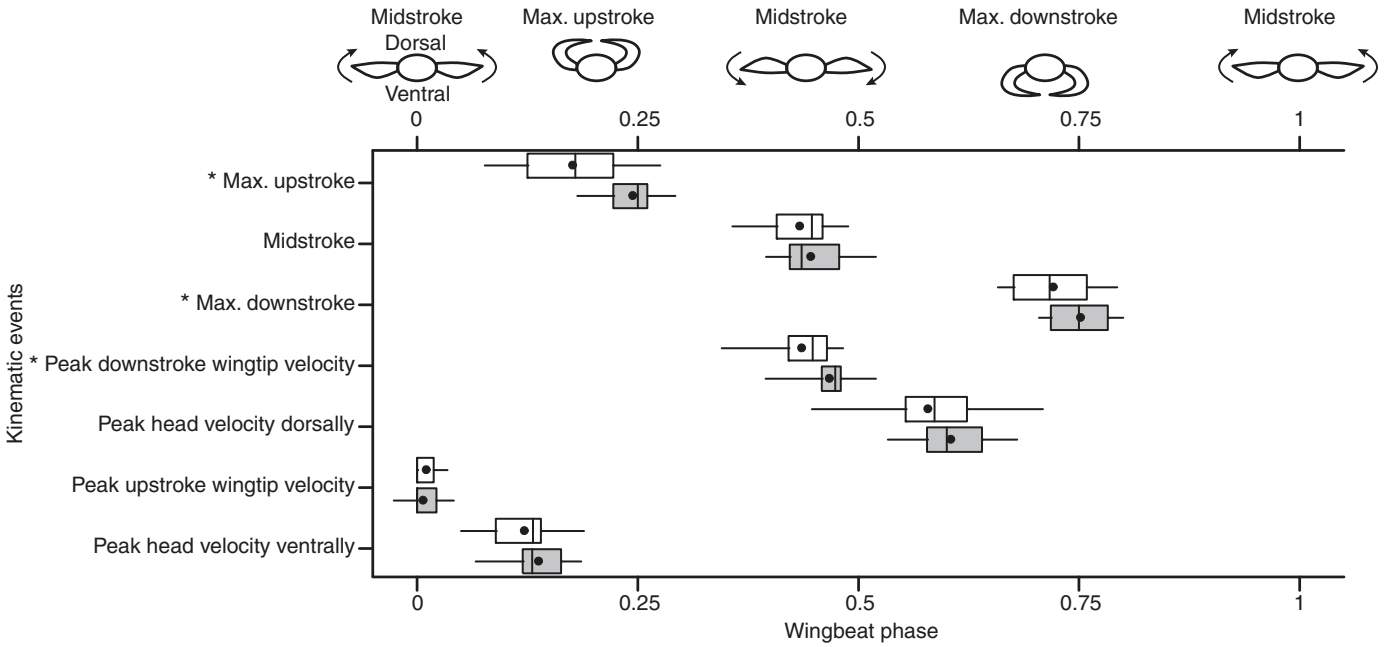

Fig. 8. Phasic timing of kinematic events during slow swimming (white boxes) and fast swimming (gray boxes). Phase 0 and phase 1 were defined by the midpoint of each wingbeat's upstroke. Cartoons (top) show a superior view of *Clione* demonstrating midstrokes and the stroke maxima; arrows indicate direction of wing motion. The central line of each box indicates the median while a dot marks the mean. The left and right edges of each box are the lower and upper quartiles, respectively, and whiskers denote the minimum and maximum observations. *P<0.01, two sample paired t-test comparing slow with fast swimming.

animals that balance their negative buoyancy and 'hover' simply translate back-and-forth and do not list over time.

Clione's wings demonstrate a notable amount of bending, particularly along their span. Spanwise bending is minimal during the power portion of the stroke and maximal as the wings approach their stroke maxima and reverse direction. Wing bending at the stroke maxima is more prominent during fast swimming, which has three possible advantages. (1) Pulling the wings closer to the body may serve as a putative squeeze mechanism to decrease drag and overcome stall (Satterlie et al., 1985). As the wings bend towards the body and reverse their angle of attack, they may force water downwards in a quasi-jet propulsive mechanism. A squeeze mechanism would not be unique: the bird wrasse employs a similar mechanism using its pectoral fins (Walker and Westneat, 1997) and shrimp use a tail flip squeeze mechanism to dramatic effect (Daniel and Meyhofer, 1989). (2) Increased wing bending during fast swimming likely decreases *Clione*'s aspect ratio, and therefore drag, during wing reversal. Given *Clione*'s low to medium *Re* even during fast swimming, decreased drag would be beneficial. (3) Increased wing bending may mean increased tension in the wing tissue that is reclaimed during the next half-stroke. It is well established in many, disparate systems that energy stored as tension in stretched tissues can be usefully reclaimed as elastic recoil (Alexander, 1991). This recoil may even take the form of a ballistic 'catapult' release (Ishikawa et al., 2005; Lappin et al., 2006). *Clione* may use wing bending to similar effect, releasing stored energy to overcome wing and fluid inertial forces and initiate the power stroke. In studying only the kinematics of the wingstroke, though, it is unclear whether the increased excursion of the wingtips during fast swimming is simply a result of their increased velocity and therefore greater momentum.

Fluid dynamics

The angle of *C. limacina*'s wing chord relative to the body's dorsal–ventral axis, γ, is similar to that of its southern hemisphere cousin, *C. antarctica*. Borrell and colleagues reported a mean midstroke chord angle of 46.0 deg in free swimming *C. antarctica* (Borrell et al., 2005). *Clione limacina*'s mean slow swimming chord angle was measured here as 44.6 deg during downstroke. Borrell and colleagues demonstrated that *C. antarctica*'s wing angle of attack increased as body velocity increased, and averaged 71.4 deg. Here, we show an increase in angle of attack with the transition to fast swimming in *C. limacina* from 63.9 deg during slow swimming downstroke to 70.1 deg during fast swimming.

At low *Re*, high wing angles such as these may indicate the use of unsteady mechanisms to generate fluid dynamic forces. Low *Re* and high angles of attack see the formation of a leading edge vortex that has been shown to greatly increase lift in *Drosophila* (Dickinson and Götz, 1993). But there is further potential for unsteady effects to contribute to force production in *C. limacina*. Maximum lift is generated by a *Drosophila* wing when it translates through the wake created by a previous wingstroke (Dickinson, 1994; Dickinson et al., 1999). In *Clione*, slow swimming often means hovering, so each half-stroke traverses directly through the path of the previous half-stroke. Wake recapture therefore has the potential to contribute significantly to lift generation in *Clione*. Dynamically scaled *Drosophila* wings operating at $Re \approx 100$ have been shown to maximize lift at α between 40 and 50 deg (Sane and Dickinson, 2001). Lift remained high in these wings until $\alpha \approx 75$ deg, at which point lift decreased as drag increased. The increased lift of high angles of attack has been attributed to vorticity shed into the wake at the end of the stroke. As these angles and *Re* values mirror those of *Clione*, it is feasible that *Clione* may employ similar unsteady mechanisms.

Clione probably uses a combination of lift-based and drag-based propulsion. *Clione*'s low *Re*, low aspect ratio, high angle of attack and low wingbeat frequency classically point to drag-based propulsion. While peak lift in *Drosophila* is produced at the stroke maxima as a result of wake recapture (Sane and Dickinson, 2002), in *Clione* the stroke maxima see tremendous spanwise bending that only increases during fast swimming (Fig. 7). This bending may mitigate *Clione*'s ability to benefit from wake recapture at the stroke maxima, though not necessarily through the entire stroke. Rotational circulation may also be mitigated by *Clione*'s wing reversal kinematics as they interact with the body and bend about their span. Spanwise vortex shedding has been shown to increase lift at slightly higher *Re* (Ellington et al., 1996), but spanwise flow within the leading edge vortex has not been observed at *Re* similar to *Clione*'s (Birch and Dickinson, 2001; Birch et al., 2004). And again, it is unclear how *Clione*'s tremendous spanwise bending might alter such flow. *Clione*'s wings likely act as drag-based paddles that also take advantage of lift-based unsteady mechanisms.

Perhaps complicating all of this, *Clione*'s wing morphology differs dramatically from the morphology of low *Re* insect wings. The molluscan parapodium is two sheets of muscle and connective tissue that enclose a fluid-filled hemocoel. The muscularized and flexible wing has a cross-section with a thick, rounded leading edge that tapers down its chord to a thin trailing edge [see previous work for detailed morphological descriptions of *Clione*'s wings (Satterlie et al., 1985; Satterlie, 1993)]. This tapering, muscularly active, flexible foil may not be well modeled by the flat, passive, rigid planforms often used to characterize insect wings. Studies of wing bending in the ratfish and in *Manduca* (operating at comparatively high *Re* values) describe wings that flex primarily near the tip and more so about the chord than the span (Combes and Daniel, 2001; Combes and Daniel, 2003a; Combes and Daniel, 2003b). *Clione*'s wings bend along their chord to varying extents during the wingbeat B.G.S., personal observation), but their spanwise bending is more dramatically apparent and occurs along the entire span. At this point, it is unclear how *Clione*'s large wing flexions may affect its low *Re* flow dynamics.

In many flapping flyers, upstroke and downstroke are asymmetrical. Downstroke acts as the power stroke, producing the driving forces, and while upstroke may produce useful force, it primarily acts as a recovery stoke, minimizing drag while positioning the wings for the next downstroke. Upstroke and downstroke asymmetry generally involves differences in the angle of attack and relative timing of the half-strokes, and stroke asymmetry has been shown in systems from low (Dickinson and Götz, 1996) to high *Re* (Drucker and Jensen, 1997; Licht et al., 2010; Tobalske, 2007; Walker and Westneat, 1997). In *Clione*, upstroke and downstroke are temporally similar. Indeed, they become more temporally equal during fast swimming as downstroke is 54.4% of the slow swim wingbeat cycle and 50.7% of the fast swim cycle (Fig. 8). This phasic symmetry of upstroke and downstroke suggests a power stroke for each half-stroke. Downstroke α averaged slightly steeper than upstroke α, but they also remain similar: slow swimming α was 63.9 deg for downstroke and 59.2 deg for upstroke; fast swimming α was 70.1 deg for downstroke and 63.0 deg for upstroke. Upstroke kinematics largely reflect downstroke kinematics and are not directly done to decrease drag as in some systems, e.g. orienting the wing parallel to the free stream. While *Clione*'s upstrokes and downstrokes are not identical and may not contribute equally to force production, their high kinematic similarity clearly points to both half-strokes contributing to swim progression.

This is not to imply that *Clione* does not engage in drag-reducing strategies, though. At the stroke maxima, the wings orient parallel to the long axis of the body (Fig. 7). As *Clione*'s swimming is progression up the water column, minimizing drag during the recovery portion of the half-stroke means minimizing the aspect ratio relative to upward movement. Pulling the wings close to the body and orienting them parallel to upward progression decreases the aspect ratio of the whole animal during wing reversal.

Gait transition

It is tempting to analogize *Clione*'s swim speeds to locomotory gaits. It is clear that *Clione*'s swim CPG is modified in order to bring about fast swimming (Arshavsky et al., 1985b; Arshavsky et al., 1989; Satterlie et al., 2000; Pirtle and Satterlie, 2004). Most studies that examine CPG modifications with respect to gaits focus on how the CPG rhythm changes the phasic timing of limb or body segment movement. Gaits are generally defined not by CPG patterns *per se* but by kinematic events like the duration of a limb's ground contact or its aerial phase (Hildebrand, 1965). CPG modifications help create the gaits, but the gaits likely evolved to minimize energy expenditure, e.g. by maximizing the storage and release of energy from elastic tissues (Biewener, 2006). While the behavior of *Clione*'s swim CPG suggests that its two-geared rhythm controls a gait transition, evidence below the level of the central nervous system may further support a two-gait claim.

At the neuromuscular level, *Clione*'s wings possess both slow twitch fatigue-resistant fibers and fast twitch fatiguable fibers (Satterlie et al., 1990). Slow twitch fibers are innervated by small motoneurons and are used during slow swimming. Fast twitch fibers are innervated by large motoneurons, presumably aiding the fibers' time to peak tension, and are recruited during the escape response and during fast swimming (Satterlie et al., 1990; Satterlie, 1991b; Satterlie, 1993). The presence of different muscle tissue types has been used as evidence of multiple gaits in fish (Webb, 1994). But the simple presence of different fiber types and the recruitment of fast twitch fibers during fast swimming are not themselves evidence of a gait transition from slow to fast swimming: slow twitch fibers may simply be unable to effect or sustain fast swimming (Rome et al., 1988).

Many aquatic systems effect gait changes by differential use of locomotory appendages. Focusing on aquatic flapping, pectoral fin rowing by fish transitions to combined pectoral–caudal fin use (Drucker, 1996), and juvenile fish transition from asynchronous left–right pectoral fin rowing to in-phase rowing, then eventually to caudal fin swimming as speed increases (Hale et al., 2006). *Clione*'s locomotory appendages do not exhibit a clear phasic kinematic change (Fig. 8) or a synchronicity change, nor is there a transition to an alternative mechanism of propulsion.

Rather than pectoral fin rowers, *Clione*'s swimming appears more similar to the mobuliform swimming of certain batoid fishes like manta rays. Whereas some batoids are rajiform swimmers that use undulatory motions of their pectoral fins to create waves on the fin, mobuliform swimmers oscillate their pectoral fins, producing less than half a wave on the fin (Rosenberger, 2001; Rosenberger and Westneat, 1999; Webb, 1994). In these oscillatory/mobuliform swimmers, increases in swim speed have been attributed to increases in the speed of the pectoral fin waves, the number of these waves, their oscillatory amplitude, and the fin-tip velocity (Rosenberger, 2001). Perhaps most telling, while batoids have different muscle types, discreet swim gaits with abrupt kinematic changes, like those changes seen in pectoral rowers or terrestrial gaits, are not seen in mobuliform swimmers (Webb, 1994).

Gait kinematics are likely determined by the internal properties of movement, evolved for energetic benefit or stability (Gatesy and Biewener, 1991; Muir et al., 1996). The increased wing bending during *Clione*'s fast swimming (Fig. 7) may be indicative of strategies employed to decrease energy expenditure at that speed by decreasing drag. And, if wing bending is used as an energy storage/release mechanism, increased wing bending would also increase the benefit of reclaiming energy stored as stretched wing tissue.

But gait kinematics are also determined by the interaction of the animal's body with its surrounding environment. Bird and bat gaits differ in the airflow patterns produced by the wings: slow flight effects a vortex-ring gait where only the downstroke of the wings produces lift, and faster flight creates a continuous-vortex gait where both downstrokes and upstrokes produce lift (Hedrick et al., 2002; Tobalske, 2007). From a fluid dynamic standpoint, the *Re* changes that take place between slow and fast swimming in *Clione* are unlikely to greatly alter the wings' flow regimes. While Re_f was nearly double Re_s in some individuals in this study, Re_f always remained firmly at the low end of the transitional range (Table 1). Indeed, numerous individuals' Re_s values exceeded the Re_f values of other individuals. *Clione* may well be an example of a two-gaited locomotory system where the central nervous system and neuromuscular machinery behave dramatically differently to create two gaits, but the phase-based kinematics of these gaits are remarkably similar because of the fact that the flow regime has not greatly changed along with the gait.

In discussing *Clione*'s two-geared swimming behavior, one cannot divorce the mechanics of the swimming from the animal's natural history. Being a negatively buoyant, pelagic creature, *Clione* constantly uses slow swimming to maintain its position in the water column. The transition from slow to fast swimming in *Clione* occurs either after a noxious stimulus (fast swimming as escape) or in response to the presence of prey (fast swimming as hunting). *Clione* does not transition from slow to fast swimming merely to increase speed – though clearly this happens – nor as a means of conserving energy while increasing speed – though energy conservation may occur. Fast swimming behavior represents a heightened state of arousal, a survival behavior; *Clione*'s fast swimming is not simply a way of increasing locomotory speed or efficiency.

Clione limacina's southern-hemisphere relative *C. antarctica* initiates a withdrawal response upon perturbation, and *C. antarctica* does not swim fast despite feeding on identical prey (Borrell et al., 2005; Gilmer and Lalli, 1990). Withdrawal is apparently an adequate defense for *C. antarctica*, and fast swimming is apparently not a requirement for its successful feeding. Rosenthal and colleagues posit that the Antarctic *Clione* has lost its fast swimming behavior as a result of evolutionary pressure on its aerobic abilities (Rosenthal et al., 2009). A physiological explanation such as this carries weight given that losing the fast swim behavior would adversely affect two separate aspects of survivability. Whatever the evolutionary history or the ecological or physiological causes, *C. antarctica* does not have the neuromuscular machinery to produce fast swimming the way *C. limacina* does (Rosenthal et al., 2009), nor is it capable of *C. limacina*'s ballistic escape response.

While there are pronounced neural modifications that take place both in the CPG and in motoneuron recruitment in order to create fast swimming in *C. limacina*, the wings end up moving in remarkably similar ways at the different speeds. Perhaps this is unsurprising: wingbeat frequency increased less than twofold between slow and fast swimming, Re_f was not dramatically greater than Re_s (Table 1), and the amplitude of *Clione*'s wing movements change little from slow swimming to fast swimming (Figs 5 and 6). One would expect minimal pressure for *Clione* to evolve different kinematic strategies for its different swim speeds if the hydrodynamic patterns of the two speeds are similar. Most of the benefits of fast swimming could be achieved by simply doing 'slow swimming faster', without the need for dramatic alterations to muscular coordination. Fluid dynamic analyses of *Clione*'s wings will cast light on how swim speed alters variables such as vortex creation, wake recapture and other unsteady mechanisms. The relative influences of such variables will help to define *Clione*'s swimming beyond simply its speed, e.g. gait selection.

Clione's neural behaviors are well understood; they effect a relatively small and reliably elicited locomotory repertoire that simplifies experimental study. *Clione*'s muscular morphology is well characterized. The flow regime of its swimming allows one to draw considerable knowledge from the literature on low to intermediate *Re* flapping flight, while at the same time obtaining insight into flexible foils. In terms of integrative biology, *C. limacina* has much to offer as a model for studying the interactions of neural control, muscular coordination and fluid dynamics.

LIST OF SYMBOLS AND ABBREVIATIONS

A	wing surface area
AR	aspect ratio ($=4L^2/S$)
c	wing chord
$\bar{c}$	mean wing chord ($=A/S$)
CPG	central pattern generator
J	advance ratio
L	wing length
n_f	wingbeat frequency during fast swimming
n_s	wingbeat frequency during slow swimming
Re_f	*Re* of mean wing chord during fast swimming
Re_s	*Re* of mean wing chord during slow swimming
S	wingspan ($=2L$)
S^1	wingspan measured from wingtip to wingtip, including the body
α	angle of attack
β	stroke plane angle
γ	wing chord angle

ACKNOWLEDGEMENTS

We thank Ranu Jung for access to her Peak Motus system and Thomas Pirtle for his tireless animal collection. The constructive comments of two anonymous reviewers substantially improved this paper.

FUNDING

Financial support was provided by a National Science Foundation IGERT fellowship to B.G.S.

REFERENCES

Abdel-Aziz, Y. I. and Karara, H. M. (1971). Direct linear transformation from comparator coordinates into object space coordinates in close-range photogrammetry. In *Proceedings from the ASP/UI Symposium on Close-Range Photogrammetry*, pp. 1-18. Urbana, Illinois: University of Illinois.

Alexander, R. (1991). Energy-saving mechanisms in walking and running. *J. Exp. Biol.* **160**, 55-69.

Antzoulatos, E. G. and Byrne, J. H. (2007). Long-term sensitization training produces spike narrowing in *Aplysia* sensory neurons. *J. Neurosci.* **27**, 676-683.

Arshavsky, Y. I., Beloozerova, I. N., Orlovsky, G. N., Panchin, Y. V. and Pavlova, G. A. (1985a). Control of locomotion in marine mollusc *Clione limacina*. III. On the origin of locomotory rhythm. *Exp. Brain Res.* **58**, 273-284.

Arshavsky, Y. I., Beloozerova, I. N., Orlovsky, G. N., Panchin, Y. V. and Pavlova, G. A. (1985b). Control of locomotion in marine mollusc *Clione limacina*. IV. Role of type 12 interneurons. *Exp. Brain Res.* **58**, 285-293.

Arshavsky, Y. I., Orlovsky, G. N., Panchin, Y. V. and Pavlova, G. A. (1989). Control of locomotion in marine mollusc *Clione limacina*. VII. Reexamination of type 12 interneurons. *Exp. Brain Res.* **78**, 398-406.

Biewener, A. A. (2006). Patterns of mechanical energy change in tetrapod gait: pendula, springs and work. *J. Exp. Zool. A Comp. Exp. Biol.* **305**, 899-911.

Birch, J. M. and Dickinson, M. H. (2001). Spanwise flow and the attachment of the leading-edge vortex on insect wings. *Nature* **412**, 729-733.

Birch, J. M., Dickson, W. B. and Dickinson, M. H. (2004). Force production and flow structure of the leading edge vortex on flapping wings at high and low Reynolds numbers. *J. Exp. Biol.* **207**, 1063-1072.

Borrell, B. J., Goldbogen, J. A. and Dudley, R. (2005). Aquatic wing flapping at low Reynolds numbers: swimming kinematics of the antarctic pteropod, *Clione antarctica*. *J. Exp. Biol.* **208**, 2399-2949.
Combes, S. A. and Daniel, T. L. (2001). Shape, flapping and flexion: wing and fin design for forward flight. *J. Exp. Biol.* **204**, 2073-2085.
Combes, S. A. and Daniel, T. L. (2003a). Flexural stiffness in insect wings. II. Spatial distribution and dynamic wing bending. *J. Exp. Biol.* **206**, 2989-2997.
Combes, S. A. and Daniel, T. L. (2003b). Into thin air: contributions of aerodynamic and inertial-elastic forces to wing bending in the hawkmoth *Manduca sexta*. *J. Exp. Biol.* **206**, 2999-3006.
Daniel, T. L. and Meyhofer, E. (1989). Size limits in escape locomotion of carridean shrimp. *J. Exp. Biol.* **143**, 245-265.
Daniel, T. L., Jordan, C. and Grunbaum, D. (1992). Hydrodynamics of swimming. In *Mechanics of Animal Locomotion* (ed. R. M. Alexander), pp. 17-49. Berlin: Springer-Verlag.
Deliagina, T. G., Arshavsky, Y. I. and Orlovsky, G. N. (1998). Control of spatial orientation in a mollusc. *Nature* **393**, 172-175.
Dickinson, M. H. (1994). The effects of wing rotation on unsteady aerodynamic performance at low Reynolds numbers. *J. Exp. Biol.* **192**, 179-206.
Dickinson, M. H. and Götz, K. G. (1993). Unsteady aerodynamic performance of model wings at low Reynolds numbers. *J. Exp. Biol.* **174**, 45-64.
Dickinson, M. H. and Götz, K. G. (1996). Wake dynamics and flight forces of the fruit fly *Drosophila melanogaster*. *J. Exp. Biol.* **199**, 2085-2104.
Dickinson, M. H., Lehmann, F.-O. and Sane, S. P. (1999). Wing rotation and the aerodynamic basis of insect flight. *Science* **284**, 1954-1960.
Drucker, E. G. (1996). The use of gait transition speed in comparative studies of fish locomotion. *Am. Zool.* **36**, 555-566.
Drucker, E. G. and Jensen, J. S. (1997). Kinematic and electromyographic analysis of steady pectoral fin swimming in the surfperches. *J. Exp. Biol.* **200**, 1709-1723.
Ellington, C. P., van den Berg, C. and Willmott, A. P. (1996). Leading edge vortices in insect flight. *Nature* **384**, 626-630.
Gatesy, S. M. and Biewener, A. A. (1991). Bipedal locomotion: effects of speed, size, and limb posture in birds and humans. *J. Zool. Lond.* **224**, 127-147.
Gilmer, R. W. and Lalli, C. M. (1990). Bipolar variation in *Clione*, a gymnosomatous pteropod. *Am. Malacol. Bull.* **8**, 67-75.
Hale, M. E., Day, R. D., Thorsen, D. H. and Westneat, M. W. (2006). Pectoral fin coordination and gait transitions in steadily swimming juvenile reef fishes. *J. Exp. Biol.* **209**, 3708-3718.
Harris-Warrick, R. M. and Marder, E. (1991). Modulation of neural networks for behavior. *Annu. Rev. Neurosci.* **14**, 39-57.
Haynes, W. M. (ed.) (2010). Properties of seawater. In *CRC Handbook of Chemistry and Physics*, pp. 14-15. Cleveland: CRC Press.
Hedrick, T. L. (2008). Software techniques for two- and three-dimensional kinematic measurements of biological and biomimetic systems. *Bioinspir. Biomim.* **3**, 1-6.
Hedrick, T. L., Tobalske, B. W. and Biewener, A. A. (2002). Estimates of circulation and gait change based on a three-dimensional kinematic analysis of flight in cockatiels (*Nymphicus hollandicus*) and ringed turtle-doves (*Streptopelia risoria*). *J. Exp. Biol.* **205**, 1389-1409.
Hildebrand, M. (1965). Symmetrical gaits in horses. *Science* **150**, 701-708.
Hoyt, D. F. and Taylor, C. R. (1981). Gait and energetics of locomotion in horses. *Nature* **292**, 239-240.
Ishikawa, M., Komi, P. V., Grey, M. J., Lepola, V. and Bruggemann, G.-P. (2005). Muscle-tendon interaction and elastic energy usage in human walking. *J. Appl. Physiol.* **99**, 603-608.
Lappin, A. K., Monroy, J. A., Pilarski, J. Q., Zepnewski, E. D., Pierotti, D. J. and Nishikawa, K. C. (2006). Storage and recovery of elastic potential energy powers ballistic prey capture in toads. *J. Exp. Biol.* **209**, 2535-2553.
Licht, S. C., Wibawa, M. S., Hover, F. S. and Triantafyllou, M. S. (2010). In-line motion causes high thrust and efficiency in flapping foils that use power downstroke. *J. Exp. Biol.* **213**, 63-71.
Muir, G. D., Gosline, J. M. and Steeves, J. D. (1996). Ontogeny of bipedal locomotion: walking and running in the chick. *J. Phys.* **493**, 589-601.
Ormshaw, J. and Elliott, C. (2006). Octopamine boosts snail locomotion: behavioural and cellular analysis. *Invert. Neurosc.* **6**, 215-220.
Pirtle, T. J. and Satterlie, R. A. (2004). Cellular mechanisms underlying swim acceleration in the pteropod mollusk *Clione limacina*. *Integr. Comp. Biol.* **44**, 37-46.
Quillin, K. J. (1999). Kinematic scaling of locomotion by hydrostatic animals: ontogeny of peristaltic crawling by the earthworm *Lumbricus terrestris*. *J. Exp. Biol.* **202**, 661-674.
Rome, L. C., Funke, R. P., Alexander, R. M., Lutz, G., Aldridge, H., Scott, F. and Freadman, M. (1988). Why animals have different muscle fibre types. *Nature* **355**, 824-827.
Rosenberger, L. J. (2001). Pectoral fin locomotion in batoid fishes: undulation *versus* oscillation. *J. Exp. Biol.* **204**, 379-394.
Rosenberger, L. J. and Westneat, M. W. (1999). Functional morphology of undulatory pectoral fin locomotion in the stingray *Taenuira lymma* (*Chondrichthyes: Dasyatidae*). *J. Exp. Biol.* **202**, 3523-3539.
Rosenthal, J. J. C., Seibel, B. A., Dymowska, A. and Bezanilla, F. (2009). Trade-off between aerobic capacity and locomotor capability in an Antarctic pteropod. *Proc. Natl. Acad. Sci. USA* **106**, 6192-6196.
Sane, S. P. and Dickinson, M. H. (2001). The control of flight force by a flapping wing: Lift and drag production. *J. Exp. Biol.* **204**, 2607-2626.
Sane, S. P. and Dickinson, M. H. (2002). The aerodynamic effects of wing rotation and a revised quasi-steady model of flapping flight. *J. Exp. Biol.* **205**, 1087-1096.
Satterlie, R. A. (1985). Reciprocal inhibition and postinhibitory rebound produce reverberation in a locomotor pattern generator. *Science* **229**, 402-404.
Satterlie, R. A. (1991a). Electrophysiology of swim musculature in the pteropod mollusc *Clione limacina*. *J. Exp. Biol.* **159**, 285-301.
Satterlie, R. A. (1991b). Neural control of speed changes in an opisthobranch locomotory system. *Biol. Bull.* **180**, 228-233.
Satterlie, R. A. (1993). Neuromuscular organization in the swimming system of the pteropod mollusc *Clione limacina*. *J. Exp. Biol.* **181**, 119-140.
Satterlie, R. A. and Norekian, T. P. (1995). Serotonergic modulation of swimming speed in the pteropod mollusc *Clione limacina*. III. Cerebral neurons. *J. Exp. Biol.* **198**, 917-930.
Satterlie, R. A. and Norekian, T. P. (2001). Mechanisms of locomotory speed change: the pteropod solution. *Am. Zool.* **41**, 1001-1008.
Satterlie, R. A., Labarbera, M. and Spencer, A. N. (1985). Swimming in the pteropod mollusc, *Clione limacina*. I. Behavior and morphology. *J. Exp. Biol.* **116**, 189-204.
Satterlie, R. A., Goslow, G. E., Jr and Reyes, A. (1990). Two types of striated muscle suggest two-geared swimming in the pteropod mollusc *Clione limacina*. *J. Exp. Zool.* **255**, 131-140.
Satterlie, R. A., Norekian, T. P. and Pirtle, T. J. (2000). Serotonin-induced spike narrowing in a locomotor pattern generator permits increases in cycle frequency during accelerations. *J. Neurophys.* **83**, 2163-2170.
Seibel, B. A., Thuesen, E. V. and Childress, J. J. (1998). Flight of the vampire: ontogenetic gait-transition in *Vampyroteuthis infernalis* (*Cephelapoda: Vampyromorpha*). *J. Exp. Biol.* **201**, 2413-2424.
Tobalske, B. W. (2007). Biomechanics of bird flight. *J. Exp. Biol.* **210**, 3135-3146.
Trimmer, B. and Issberner, J. (2007). Kinematics of soft-bodied, legged locomotion in *Manduca sexta* larvae. *Bio. Bull.* **212**, 130-142.
Walker, J. A. and Westneat, M. W. (1997). Labriform propulsion in fishes: Kinematics of flapping aquatic flight in the bird wrasse *Gomphosus varius* (*Labridae*). *J. Exp. Biol.* **200**, 1549-1569.
Watson, W. H., III, Newcomb, J. M. and Thompson, S. (2002). Neural correlates of swimming behavior in *Melibe leonina*. *Biol. Bull.* **203**, 152-160.
Webb, P. W. (1994). The biology of fish swimming. In *Mechanics and Physiology of Animal Swimming* (ed. L. Maddock, Q. Bone and J. M. V. Rayner), pp. 45-62. Cambridge: Cambridge University Press.
Willows, A. O. D. and Hoyle, G. (1969). Neuronal network triggering a fixed action pattern. *Science* **166**, 1549-1551.